Submitted to the Astrophysical Journal
Preprint typeset using LaTeX style emulateapj v. 6/22/04



# NEAR-INFRARED AND OPTICAL LIMITS FOR THE CENTRAL X-RAY POINT SOURCE IN THE CASSIOPEIA A SUPERNOVA REMNANT[1]

R. A. Fesen[2], G. G. Pavlov[3] & D. Sanwal[3]

(Received 2005 June 28)
*Submitted to the Astrophysical Journal*

## ABSTRACT

We set new near-infrared and optical magnitude limits for the central X-ray point source (XPS) in the Cassiopeia A supernova remnant based on *HST* images. Near-infrared images of the center of Cas A taken with the NICMOS 2 camera in combination with the F110W and F160W filters ($\sim$ J and H bands) have magnitude limits $\geq$26.2 and $\geq$24.6, respectively. These images reveal no sources within a 1.″2 radius (corresponding to a 99% confidence limit) of the *Chandra* XPS position. The NICMOS data, taken together with broadband optical magnitude limits ($R \sim 28$ mag) obtained from a deep STIS CCD exposure taken with a clear filter (50CCD), indicate that the XPS luminosities are very low in the optical/NIR bands (e.g., $L_H < 3 \times 10^{29}$ erg s$^{-1}$) with no optical, J, or H band counterpart to the XPS easily detectable by *HST*. The closest detected object lies 1.″8 from the XPS's nominal coordinates, with magnitudes $R = 25.7$, $m_{\rm F110W} = 21.9$, and $m_{\rm F160W} = 20.6$, and is a foreground, late-type star as suggested by Kaplan, Kulkarni, & Murray. We discuss the nature of the Cas A central compact object based upon these near-infrared and optical flux limits.

*Subject headings:* ISM: individual (Cassiopeia A) — supernova remnants — stars: neutron — X-rays: stars

## 1. INTRODUCTION

Cassiopeia A (Cas A) is a $\sim$300 yr old supernova remnant (SNR) containing high-velocity ejecta exhibiting O and Si-group abundances like those expected from the supernova of massive star (Chevalier & Kirshner 1978, 1979; van den Bergh & Kamper 1983; Tsunemi et al. 1986; Jansen et al. 1988; Douvion et al. 1999; Thorstensen et al. 2001). Because it is the best known member of the class of remnants from high-mass, core-collapse supernovae, it has been the target of several investigations looking for a possible compact stellar remnant near its expansion center (Kamper & van den Bergh 1976; van den Bergh & Pritchet 1986; Woan & Duffett-Smith 1993; Lorimer et al. 1998).

None of these searches were successful until first-light images of Cas A taken in 1999 by the *Chandra* X-ray Observatory revealed a central X-ray point source (XPS) (Tananbaum 1999). Re-examinations of archival *ROSAT* and *Einstein* X-ray data (Aschenbach 1999; Pavlov & Zavlin 1999) showed that this X-ray point source had actually been detected much earlier but was not realized as such until the *Chandra* higher resolution images clarified the spatial structure of the Cas A's central region.

A blackbody fit to the observed *Chandra* Advanced CCD Imaging Spectrometer (ACIS) spectrum shows a high temperature $kT \approx 0.5$ keV and a small effective radius $R \approx 0.4$ km, at the remnant's estimated distance of 3.4 kpc (Reed et al. 1995), leading to suggestions of a neutron star with hot spots (Pavlov et al. 2000). Analysis of a recent 1 Ms *Chandra* image of Cas A shows no extended pulsar wind nebula around the point source (Hwang et al. 2004).

Although ostensibly the remnant's central compact object (CCO), the nature of Cas A's XPS remains uncertain. The observed X-ray emission could arise either from a young but radio-quiet neutron star or an accretion disk around a black hole or neutron star. Soon after its discovery, Pavlov et al. (1999) and Chakrabarty et al. (2001) suggested it might be related to the class of slowly rotating neutron stars known as Anomalous X-ray Pulsars (AXPs) and Soft Gamma Repeaters (SGRs). AXPs and SGRs are radio-quiet, exhibit relatively long periods of several seconds and occasional outbursts, and are thought to have extremely strong magnetic fields, $\sim 10^{14}$–$10^{15}$ G. Several AXPs have been associated with SNRs (Mereghetti et al. 2002a; Gaensler 2004) and a mid-$20^{th}$ century SGR flare from the Cas A XPS has been proposed as the source of apparent 24$\mu$ light echo filaments located $\sim 20'$ north and south of the remnant seen in *Spitzer* and ground-based $K_s$ band images (Krause et al. 2005). However, X-ray period searches on Cas A's XPS have been unsuccessful so far (Chakrabarty et al. 2001; Mereghetti, Tiengo, & Israel 2002b).

Several deep radio, infrared, and optical searches for central compact object have been conducted both before and after discovery of the XPS, all without success. No radio pulsar has been detected at the XPS's position down to 30 mJy and 1.3 mJy at 327 and 1435 MHz, respectively (McLaughlin et al. 2001), and there is no Infrared Space Observatory (*ISO*) detected IR source near the remnant's center (Lagage et al. 1996). Deep ground-based optical and near-infrared (NIR) searches have detected only one candidate near the *Chandra* XPS posi-

[1] Based on observations with the NASA/ESA Hubble Space Telescope, obtained at the Space Telescope Science Institute, which is operated by the Association of Universities for Research in Astronomy, Inc. under NASA contract No. NAS5-26555. These observations are associated with programs GO-8692 and GO-9798.

[2] 6127 Wilder Lab, Department of Physics & Astronomy, Dartmouth College, Hanover, NH 03755; fesen@snr.dartmouth.edu
[3] The Pennsylvania State University, 525 Davey Lab., University Park, PA 16802; pavlov@astro.psu.edu, divas@astro.psu.edu

tion ($m_{\rm F675W}$ = 26.7, $J$ = 21.4, $H$ = 20.5, $K_s$ = 20.5; Kaplan, Kulkarni, & Murray 2001). However, this object appears to be a foreground Pop II star (Kaplan et al. 2001). Consequently, current optical and NIR limits (see Table 1) indicate an X-ray to optical flux ratio greater than a few hundred, thereby excluding some types of accreting binary systems but not single neutron stars.

Here we report on deep NIR *Hubble Space Telescope* (*HST*) images of the Cas A XPS region using the Near Infrared Camera and Multi-Object Spectrograph (NICMOS). We also present a more complete description and analysis of broadband *HST* optical images obtained with the Space Telescope Imaging Spectrograph (STIS) (Fesen et al. 2002). Combined, these data represent the deepest optical and NIR searches for a counterpart to the Cas A XPS to date, and we discuss the implications of these non-detections on the nature of the X-ray source.

## 2. OBSERVATIONS

### 2.1. *Near-Infrared Images*

NICMOS Camera 2 (NIC2; field of view [FOV] of 19.″2 × 19.″2; 0.″075 pixel$^{-1}$) was used to image the central region of Cas A during two separate pointings in 2004 March 3–7 and 2004 June 23–24. The images were obtained using the F110W ('NICMOS J') filter ($\lambda_{\rm central}$ = 1.1 $\mu$m, bandpass = 0.8 – 1.4 $\mu$m) and F160W ('NICMOS H') filter ($\lambda_{\rm central}$ = 1.6 $\mu$m, bandpass = 1.4 – 1.8 $\mu$m). Both F110W and F160W images were obtained using a NICMOS sequence of Step=32, Nsamp=25 and a nine-point, spiral dither pattern, with an exposure time of 576 s per pointing. A three-orbit, continuous viewing zone (CVZ) observation in March 2004 resulted in a total F160W exposure of 15,550 sec. Because of a NICMOS software error, F110W data were obtained on only one of five planned CVZ orbits in March 2004. The full five-orbit F110W observations were then repeated in June 2004. However, the passages through the South Atlantic Anomaly (SAA) during the June observations caused a very high cosmic ray background. We corrected the SAA affected F110W data using the *saa_clean*[4] tool provided by STScI. The total exposure in the F110W band (one CVZ orbit in March and five CVZ orbits in June) was about 31,000 sec.

Coordinates on the NIC2 images were matched to those of the STIS CCD images (see §2.2) by manually matching three stars on each image set. The data were reduced using IRAF/STSDAS[5] routines. Measured F110W and F160W fluxes were converted to photometric magnitudes on the Vega system using NICMOS photometric keywords and Vegamag zeropoints for 77.1 K detector temperatures from current on-line NIC2 tables[6].

### 2.2. *Optical Images*

A series of five STIS CCD 52″ × 52″ images (0.″05 pixel$^{-1}$) using the clear "50CCD" filter ($\lambda_{\rm center}$ = 585 nm, FWHM = 440 nm) with a total exposure time of 12,402 sec was obtained in January 2001 covering the central region of the Cas A SNR (Fesen et al. 2002). The data were taken using a standard STIS CCD dither pattern and reduced using IRAF/STSDAS reduction programs.

Coordinates of sources detected on the STIS images were measured through the matching of these sources with those obtained from ground-based images which were placed on a World Coordinate System (WCS) based on the USNO-A2.0 catalog (Monet et al. 1998) in the same manner as described in Thorstensen, Fesen, & van den Bergh (2001). Resulting star positions on a 8′ × 8′ FOV MDM Observatory 2.4 m R band image (2 × 720 s exposures) taken in October 1999 were then checked using four Tycho-2 stars detected on the image. This resulted in a coordinate registration with the International Coordinate Reference System (ICRS) to within 0.″2. Using the ICRS catalog of reference star positions, we identified three stars on the STIS image that were then calibrated to the same zero-point of the coordinate grid.

Figure 1 shows the STIS CCD FOV marked on a 1999 MDM 2.4 m R-band image of Cas A. The exact positioning of the STIS images was dictated by an attempt to avoid scattered light problems from relatively bright stars surrounding the X-ray point source position. In addition, in order to go as deep as possible, the data were taken in "Low-Sky" mode. This mode minimizes Zodiacal Light which is the principal background source for wavelengths longer than 3500 Å. Low-Sky mode requires the data to be taken at a time during the year when the Zodiacal Light is no more than 30% greater than the minimum value for the Zodiacal Light for the target.

The STIS 50CCD filter has a very broad effective bandpass, with significant response from 250 to 1000 nm with a peak near 585 nm. Consequently, STIS 50CCD magnitudes have little direct color information and are sometimes translated into a standard filter set by quoting the result as a V magnitude. Knowledge of an object's intrinsic spectrum is required for an accurate conversion to any standard filter system and various conversion techniques have been used (Rejkuba et al. 2000; Nakamura et al. 2001; Sollerman et al. 2002). Considering the large extinction toward the remnant ($A_V$ = 5 − 6 mag; Hurford & Fesen 1996), which might be even greater toward remnant center (Troland et al. 1985), we have made use of previous R magnitude estimates of field stars in the STIS CCD FOV to calibrate the STIS data assuming an AB zeropoint of 26.39 mag.

## 3. POSITION OF THE X-RAY POINT SOURCE

A fundamental aspect of searching for an optical or NIR counterpart involves knowing the precise XPS coordinates along with a positional error radius at a given confidence level. Table 2 lists the position of the XPS as cited by Tananbaum (1999), Kaplan et al. (2001), and Murray et al. (2002). The optical and NIR search by Kaplan et al. (2001) adopted an XPS position different from that cited by Tananbaum (1999). Kaplan et al. (2001) found one star (Star A) within their quoted 90% confidence level circle (radius = 2.″3). Below, we attempt to refine the XPS's coordinates using more recent *Chandra* data.

WCS positions on *Chandra* HRC and ACIS images are

[4] `http://www.stsci.edu/hst/nicmos/tools/post_SAA_tools.html`

[5] IRAF is distributed by the National Optical Astronomy Observatories, which is operated by the Association of Universities for Research in Astronomy, Inc. (AURA) under cooperative agreement with the National Science Foundation. The Space Telescope Science Data Analysis System (STSDAS) is distributed by the Space Telescope Science Institute.

[6] `http://www.stsci.edu/hst/nicmos/performance/photometry`

believed to be good to about $\pm 0\farcs6$ (for sources observed close to the aim point) as judged from comparisons of Tycho-2 and ICRS sources on *Chandra* images (CXO manual). Based on 135 target pointings, ACIS-S positions are the most reliable (vs. ACIS-I, HRC-S, and HRC-I), with a resulting 90% confidence radius of $0\farcs55$ (T. Aldcroft, priv. comm.). Positional analysis of HRC-S and HRC-I *Chandra* images have been found to have 90% confidence radii similar to that of the ACIS-S, namely $0\farcs65$ and $0\farcs52$, but measured from fewer pointings (63 and 30, respectively; T. Aldcroft, priv. comm.).

In Table 2, we list XPS coordinate values derived from several ACIS and HRC exposures. The HRC positions include small corrections to the normal data pipeline reduction caused by small aspect offsets (M. Juda, priv. comm.). Applying these corrections, the positions of the XPS derived from the three HRC and two ACIS images all agree within $0\farcs5$.

As an additional check, we have compared our optical coordinate grid directly with that of the Cas A *Chandra* observations through an examination of the recent 1 Ms exposure from the *Chandra* Very Large Program (VLP) ACIS-S observation of the Cas A remnant (Hwang et al. 2004) on which a few weak point sources appear visible around and outside the remnant. Most of the point sources on 1 Ms image were close to optical stars, and we manually matched three of these point sources to stars on our optical reference grid. Table 3 lists these three reference point sources manually matched, three other optical sources in the USNO-A2.0 catalog of astrometric stars (Monet et al. 1998) which subsequently were found to match X-ray point sources within $1''$ in the combined 1 Ms *Chandra* ACIS image using our plate solution, plus three additional sources that matched optical stars (one bright and two faint) on our reference MDM 2.4 m R-band image. The resulting uncertainty of $0\farcs6$ includes the systematic uncertainty of the USNO-A2.0 catalog (Monet et al. 1998), the $0\farcs2$ registration error between the MDM image, and the USNO catalog (Thorstensen et al. 2001), and measurement uncertainty of the XPS on the 1 Ms exposure due to an asymmetric point spread function. Our measured position for the XPS using this revised WCS 1 Ms ACIS-S image is listed near the bottom of Table 2 and is in agreement with the mean of HRC and ACIS derived positions.

Based on this and the ACIS and HRC positional data, we adopted a XPS position of $\alpha$(J2000) = $23^{\rm h}\ 23^{\rm m}\ 27\fs943$, $\delta$(2000) = $58^{\rm o}\ 48'\ 42\farcs51$ with an $1\sigma$ uncertainty of $0\farcs4$ (see Table 2). Ironically, this position is in excellent agreement with the initial XPS coordinates quoted by Tananbaum (1999) based only on short (a few ks) first-light *Chandra* images.

## 4. RESULTS AND ANALYSIS

### 4.1. *Optical and NIR Flux Limits for the XPS*

The combined STIS 50CCD image of the central region of Cas A roughly centered on the XPS coordinates is shown in the upper left hand panel of Figure 2. The location of the remnant's center of expansion as determined by Thorstensen et al. (2001) is also shown, some $6\farcs6$ to the north. Two faint stars located $6''$ – $7''$ west of the XPS coordinates are labeled '1' and '2' in this figure.

The upper right hand panel of Figure 2 shows a blowup of the STIS image with 95% confidence circles (radii = $0\farcs9$) centered on the XPS position as determined from the ACIS and HRC data. The image shows only one prominent star near the *Chandra* error circles. This Star A, discussed by Kaplan et al. (2001), has a quoted WFPC2 F675W magnitude $m_{\rm F675W} = 26.7 \pm 0.2$ and lies outside both 95% confidence circles. Based on the star's colors, Kaplan et al. (2001) argue that it is likely a foreground late M star, not associated with the XPS.

No other object was detected within or close to the *Chandra* error circle in the combined STIS 50CCD image. Adopting the Ryan, Wagner, & Starrfield (2001) quoted $R = 24.7$ mag for Star 2 located about $7''$ northwest of the X-ray point source's position (see their Fig. 2) and a WFPC2 F675W magnitude of 26.7±0.2 for Star A from Kaplan et al. (2001), then from our estimated STIS 50CCD $3\sigma$ limit of 28.5 mag for the XPS (Vega magnitude system), we estimate a limit of $m_{\rm F675W} \geq 28.9$ and $R \geq 27.8$ mag. A $m_{\rm F675W} - R$ difference of $\simeq +1.1$ mag is in line with the expected difference for red objects (e.g., a source with a $B - V = 1.7$ mag; see the WFPC2 Cookbook). Our derived R magnitudes have uncertainties of around ±0.3 mag due to the unknown spectrum of the XPS. These detection limits also apply to any optical emission associated with the remnant's center of expansion located nearly $7''$ north of the XPS (Thorstensen et al. 2001).

The NICMOS F110W and F160W images are shown in the two lower panels of Figure 2. The error circles shown are centered on our adopted XPS position (see Table 2). Although we detected some very faint sources in the vicinity of XPS (in particular Star B $1\farcs9$ south of the XPS), we found no sources within a $1\farcs2$ radius circle corresponding to a 99% confidence limit from the adopted *Chandra* XPS position based on several measurements (see §3). We estimate the $3\sigma$ upper limits on average fluxes of 0.06 and 0.15 $\mu$Jy in the F110W and F160W bands, respectively, corresponding to F110W and F160W magnitudes limits of 26.2 and 24.6 (Vega system).

Optical and NIR magnitudes for stars near the XPS position are given in Table 4. Also listed are our estimated R, F110W, and F160W magnitudes limits for the XPS based on these STIS and NICMOS images, along with the $K_s$ band limit from Kaplan et al. (2001). The NICMOS data, taken together with the deep optical magnitude limits from the earlier STIS observations ($R \gtrsim 28$ mag) indicate that there is no optical, J band, or H band counterpart to the XPS easily detectable by *HST*.

### 4.2. *Comparison of NIR, Optical, and X-Ray Fluxes*

The properties of the central compact object in Cas A can be constrained by both its X-ray emission spectrum and through comparison of X-ray, optical, and NIR fluxes and luminosities. While comparison of uncorrected (absorbed) X-ray, optical, and NIR fluxes is fairly straightforward, analysis of multiple ACIS observations of Cas A has shown somewhat different observed XPS's flux values: e.g., from 8 to 9 $\times 10^{-13}$ erg cm$^{-2}$ s$^{-1}$ in the 0.6–6 keV band. Because the 0.6–6 keV band is where most of the detected photons are thus giving the most accurate characterization of the observed source flux, the reported scatter is most likely associated with systematic uncertainties for different observational setups and uncertain pile-up corrections, which are significant at the

observed ACIS-S count rate of about 0.35 counts per frame (Teter et al. 2005). We adopt $F_{\rm X} = 8 \times 10^{-13}$ erg cm$^{-2}$ s$^{-1}$ for the XPS's observed X-ray flux. The observed (absorbed) magnitudes limits listed in Table 4 then yield the following flux ratios: $F_{\rm X}/F_{\rm R} > 25000$, $F_{\rm X}/F_{\rm F110W} > 8400$, $F_{\rm X}/F_{\rm F160W} > 11000$, $F_{\rm X}/F_{K_s} > 1700$.

To compare extinction corrected (unabsorbed) X-ray and IR-optical luminosities, knowledge of the amount of interstellar extinction is required. Optical, radio, and X-ray measurements indicate the interstellar extinction toward Cas A appears to be large and non-uniform, with a tendency for increased absorption going from the northeast to the west and southwest (Troland et al. 1985; Keohane et al. 1996; Willingale et al. 2002). The optical extinction, $A_{\rm V}$, along the remnant's northern rim based on optical spectra of ejecta and circumstellar knots ranges from 4.6 to 6.2 mag, with the largest value found farthest off the northern rim and about halfway toward the remnant center (Hurford & Fesen 1996). Adopting $A_{\rm V} = N_{\rm H}/1.8 \times 10^{21}$ cm$^{-2}$ for a typical gas-to-dust ratio (Bohlin, Savage, & Drake 1978; Predehl & Schmitt 1995), an $A_{\rm V}$ value of 6.2 mag yields an $N_{\rm H,22} \equiv N_{\rm H}/10^{22}\,{\rm cm}^{-2} = 1.1$.

However, X-ray and radio measurements suggest that larger column densities are more common across other sections of the remnant and may be more appropriate for the remnant's central region. X-ray measurements of the remnant's overall emission spectrum suggest $N_{\rm H,22}$ values ranging from 0.9 to 2.5 (Hughes et al. 2000; Willingale et al. 2002), corresponding to $A_{\rm V}$ values of 5 – 14 mag, with $N_{\rm H,22}$ values around 1.4 – 1.5 ($A_{\rm V} = 7.8$ – 8.3) near the eastern limb (Hwang & Laming 2002). Troland et al. (1985) used H I and CO observations to estimate $A_{\rm V}$ values of $4 - 5$ mag for the northern rim, $5 - 6$ mag for most of the remnant, a value of 7.3 mag near the center, and as much as 8 mag or more along the western boundary.

More recent radio observations of the 6 cm $H_2CO$ transition (Reynoso & Goss 2002) show clumpy molecular gas toward (and maybe coincident with) the remnant, again with signs of a significant increase of the $H_2$ column density toward the western edge of the remnant. Reynoso & Goss (2002) also find a $H_2$ column density of $5.7 \times 10^{21}$ cm$^{-2}$ for a small molecular cloud just east of the remnant's expansion center (Thorstensen et al. 2001), from which they estimate $N_{\rm H,22} = 1.3$ ($A_{\rm V} = 7.2$ mag). The outskirts of this cloud may extend over to the XPS position. If correct, then this $N_{\rm H}$ value when added to the absorption of the local arm ($1.3 \times 10^{21}$ cm$^{-2}$; $A_{\rm V} = 0.7$ mag) suggests a total $A_{\rm V}$ value as high as 8 mag (Reynoso & Goss 2002) toward the XPS.

Based on the above estimates, we adopt $A_{\rm V} = 6$ – 8 mag as a plausible range for the optical extinction toward the XPS. For $A_{\rm V}/E({\rm B–V}) = 3.1$, this converts to $A_{\rm R} = 4.5 - 6.0$, $A_{\rm J} = 1.7 - 2.2$, $A_{\rm H} = 1.0 - 1.4$, and $A_{\rm K} = 0.6 - 0.9$. Assuming for instance $A_{\rm V} = 7$, we obtain the following upper limits on NIR-optical luminosities: $L_{\rm opt/NIR} < 5.6$, 0.8, 0.3, and $1.3 \times 10^{30}$ erg s$^{-1}$ for the R, F110W, F160W, and $K_s$ bands, respectively (for $d = 3.4$ kpc).

$N_{\rm H}$ values can be estimated directly from fitting the X-ray spectra, but the results are very sensitive to the choice of spectral model. Fits with blackbody models yield lowest column densities, $N_{\rm H,22} = 0.6$ – 1.2 in different data sets, and lowest unabsorbed fluxes, $F_{\rm X}^{\rm unabs} = (1.2$ – $1.4) \times 10^{-12}$ erg cm$^{-2}$ s$^{-1}$ in the 0.6 – 6 keV band. Power-law fits yield highest values for both the column density and the unabsorbed flux: $N_{\rm H,22} = 1.8$ – 2.6, $F_{\rm X}^{\rm unabs} = (8$ –12$) \times 10^{-12}$ erg cm$^{-2}$ s$^{-1}$ in the same band. Fits with more complicated models (neutron star atmospheres, blackbody plus power law, etc) yield intermediate values, typically $N_{\rm H,22} = 1.0$ – 1.2 and $F_{\rm X}^{\rm unabs} = (1.2$ – $1.6) \times 10^{-12}$ erg cm$^{-2}$ s$^{-1}$, corresponding to the isotropic 0.6–6 keV luminosity $L_X = 4\pi d^2 F_{\rm X}^{\rm unabs} = (1.7$ – $2.2) \times 10^{33}$ erg s$^{-1}$.

Unfortunately, it is currently unknown which of the models is more appropriate for the XPS since the true shape of its X-ray spectrum is not completely certain because of CCD pile-up corrections. However, the spectrum is likely to be either thermal or at least has a thermal component which favor intermediate $N_{\rm H}$ values, $N_{\rm H,22} = 1.1$ – 1.4, corresponding to $A_{\rm V}$ values of 6 – 8 (for a typical gas-to-dust ratio) and entirely consistent with the optically derived absorption estimates discussed above.

Therefore, assuming $A_{\rm V} = 7$ and $L_X = 2 \times 10^{33}$ erg s$^{-1}$ for the 0.6 – 6 keV energy range, we obtain the following ratios of X-ray to optical/NIR unabsorbed luminosities: $L_X/L_{\rm R} > 360$, $L_X/L_{\rm F110W} > 2500$, $L_X/L_{\rm F160W} > 6700$, and $L_X/L_{\rm K_s} > 1600$.

## 5. THE NATURE OF THE CAS A XPS

Analyzes made soon after the discovery of the Cas A XPS indicated that it was unlikely to be an active pulsar. There was no detected radio pulsation or $\gamma$-ray emission, no X-ray or radio plerion, and the observed X-ray spectrum appeared too steep for an ordinary pulsar (Pavlov et al. 2000). We will show below that the deep optical-NIR upper limits reported above support this conclusion.

Optical and X-ray emission of an active pulsar is characterized by a nonthermal (presumably synchrotron) component emitted from the pulsar's magnetosphere which dominates at harder X-rays and longer optical-NIR wavelengths while the main contribution from the thermal component is in the UV and soft X-rays. An example of a pulsar's NIR to X-ray spectrum is shown in the middle panel of Figure 3 for PSR B0656+14 (Pavlov et al. 2002b; Kargaltsev & Pavlov 2005), one of few pulsars showing thermal emission in both soft X-rays and the UV. For this pulsar, the nonthermal component, which dominates at $E \gtrsim 2$ keV and $\lambda > 2000$ Å, has about the same spectral slope in the hard X-rays as in the NIR-optical (photon index $\Gamma \approx 1.5$), with ratios of the nonthermal $0.6 - 6$ keV X-ray luminosity to NIR luminosities of $L_X/L_{\rm F110W} \approx 200$ and $L_X/L_{\rm F160W} \approx 400$. In other young pulsars such as the Crab pulsar, NIR and optical fluxes may lie below the continuation of the (steeper) X-ray nonthermal spectrum, but the ratios of the nonthermal X-ray-to-optical luminosities are almost the same, at a level of about a few hundred (Zavlin & Pavlov 2004).

The Cas A XPS could either have a pure thermal spectrum, which would support the assertion that it is not an active pulsar, or it may have a nonthermal power-law

component dominating above 4–5 keV with a slope $\Gamma \approx 2$ and a 0.6–6 keV unabsorbed flux $\sim 2 \times 10^{-13}$ erg cm$^{-2}$ s$^{-1}$ corresponding to $L_X \sim 3 \times 10^{32}$ erg s$^{-1}$ (Teter et al. 2005). However, an extension of this component into the optical-NIR range lies well above our upper limits (see Fig. 3). Moreover, the lower limits on the ratios of nonthermal $0.6-6$ keV X-ray and NIR/optical luminosities (e.g., $L_X/L_{\rm F110W} \gtrsim 370$, $L_X/L_{\rm F160W} \gtrsim 1000$) are somewhat higher than observed in active pulsars.

If the Cas A XPS is a neutron star, the lack of manifestations of pulsar activity can be used to constrain its parameters. Assuming the characteristic age of a putative pulsar, $\tau = P/2\dot{P}$, is close to its actual age, $\approx 1 \times 10^{10}$ s for Cas A, we obtain $P = (2\pi^2 I/\tau\dot{E})^{1/2} \approx 1.4\,\dot{E}_{36}^{-1/2}$ s, $\dot{P} \approx 6.8 \times 10^{-11}\dot{E}_{36}^{-1/2}$, and $B_p = 6.4 \times 10^{19}(P\dot{P})^{1/2} = 6.2 \times 10^{14}\dot{E}_{36}^{-1/2}$ G, where $I \simeq 10^{45}$ g cm$^2$ is the moment of inertia, $\dot{E} = 10^{36}\dot{E}_{36}$ erg s$^{-1}$ is the pulsar's spindown energy loss rate, and $B_p$ is a conventional estimate on the magnetic field at the neutron star's magnetic pole.

Based on the observed correlation between the pulsar optical luminosity and spin-down energy loss rate (e.g., Zharikov et al. 2004), our NIR-optical limits on the XPS's radiation imply a conservative upper limit $\dot{E} < 10^{37}$ erg s$^{-1}$, similar to the limit that follows from the lack of the pulsar wind nebula (Gotthelf 2004). Such a limit translates into $P > 0.4$ s, $\dot{P} > 2 \times 10^{-11}$, and $B_p > 2 \times 10^{14}$ G. This suggests that the XPS might be a slowly rotating neutron star with a very high magnetic field. (Note: The field could be lower than the above estimate if the XPS was born as slow rotator.)

Fits of the XPS's X-ray spectrum with a blackbody model show that the emitting area, $\sim 1$ km$^2$, is too small and the temperature, $\approx 6 \times 10^6$ K, too high for a $\sim 300$ yr old neutron star (Pavlov et al. 2000). The small size of the emitting area initially hinted that it might be a strongly magnetized neutron star accreting matter, possibly from a secondary companion in a binary, albeit with a very low accretion rate, $\dot{M} \sim 10^{13}$ g s$^{-1}$. However, the *HST* optical and NIR observations described above now place tight constraints on companion's absolute magnitudes. Adopting $D = 3.4$ kpc and $A_V = 7$ mag, the STIS and NICMOS magnitude limits imply $M_R \geq 10$, and $M_{F110W} \geq 11.5$, $M_{F160W} \geq 10.7$, fainter than any main-sequence star, let alone secondary components of known X-ray binaries (van Paradijs & McClintock 1995). The same argument virtually excludes accretion onto a black hole in a binary.

The observed X-ray luminosity of the XPS is also too high to be explained via accretion from the interstellar medium. At the $\simeq 300$ km s$^{-1}$ velocity derived from the displacement of the XPS from the SNR's expansion center (Thorstensen et al. 2001) and a $\sim 300$ yr age for the SNR, an unrealistically high ISM density around $10^5$ cm$^{-3}$ is needed to obtain the required accretion rate (Pavlov et al. 2000).

On the other hand, it is possible that accretion onto the central compact object might occur, not from a secondary companion or from the ISM, but from a hypothesized "fossil accretion disk" consisting of debris left over from the supernova explosion (e.g., van Paradijs, Taam, & van den Heuvel 1995; Ekşı et al. 2005, and references therein). Formation of an ejecta accretion disk due to fallback material around the neutron star sometime after the supernova explosion could give rise to NIR emission due to X-ray irradiation and/or viscous energy dissipation (Chatterjee, Hernquist, & Narayan 2000; Perna, Hernquist, & Narayan 2000; Ekşı & Alpar 2003). Such a disk might be identifiable by exhibiting NIR and optical colors substantially different from stellar ones. However, if the XPS's X-ray luminosity is due to accretion from the disk onto the neutron star surface, the corresponding accretion rate, $\dot{M} \sim 10^{13}$ g s$^{-1}$, implies a very low disk mass, $M_d(t) \sim (16/3)\dot{M}t \sim 3 \times 10^{-10} M_\odot$ at the present age $t \sim 10^{10}$ s in the disk model considered by Perna et al. (2000). Such a small disk would hardly be detectable even in very deep NIR observations.

A strong argument against any sort of accretion as being the chief source of the XPS's X-ray emission is the lack of noticeable variability. Teter et al. (2004) have analyzed *Chandra* observations of the Cas A XPS spanning a range of 4.5 years and found no statistically significant flux changes, usually observed in accreting X-ray sources. Consequently, accretion, regardless of the source of material, would seem to be an unlikely source of the observed X-ray emission.

It has been suggested that the Cas A XPS may be simply a more youthful and less luminous example of the isolated neutron star subclasses known as Anomalous X-ray Pulsars (AXPs) and Soft Gamma-ray Repeaters (SGRs) (Chakrabarty et al. 2001; Mereghetti, Tiengo, & Israel 2002b; Pavlov et al. 2002a, 2004; Rothschild & Lingenfelter 2003). Occasional bursts from AXPs and SGRs as well as their spin-down rates have been successfully explained by a magnetar model (Duncan & Thompson 1992; Thompson & Duncan 1996), in which a neutron star has a surface magnetic field of $10^{14}-10^{15}$ G. Except for a lack of pulsations, the general properties of the Cas A XPS and other CCOs in fairly young SNRs are not all that dissimilar from AXPs and SGRs. The fact that there are at least two cases of AXPs associated with SNRs (Gaensler 2004) might indicate that CCOs and AXPs are related.

AXPs exhibit X-ray spectra similar to those observed for CCOs, including the Cas A XPS (Pavlov et al. 2002a,2004), and show X-ray pulsations with periods in the range of 5–12 s. So far, however, no pulsations have been found for the Cas A XPS. The Murray et al. (2001) claim for a 12.5 ms period from the *Chandra* HRC observations was based on a low significance ($2.5\sigma$) signal, and it was not confirmed in a follow-up HRC observation (Ransom 2002). Moreover, a neutron star with a period as short as this would be an active pulsar even if it had a very low magnetic field, $\sim 3 \times 10^8$ G, and it would be hard to explain the origin of this periodicity if the field is even lower than that.

While at least four of the seven firmly established AXPs have now been detected in the optical/NIR, no CCO in a young SNR has yet been seen. Table 5 lists the observed optical (R band) and NIR (JHK$_s$) magnitudes or limits for the Cas A CCO along with five other SNRs with radio-quiet, X-ray emitting CCOs. Remnants with CCOs similar to that of Cas A are Puppis A (G260.4−3.4), the *ROSAT* discovered remnant G266.2−1.2 (sometimes called 'Vela Junior' due to its

location near the Vela SNR), and G347.3−0.5. The CCOs in G296.5+10 and Kes 79, for which short periods have been recently detected (Zavlin et al. 2000; Zavlin, Pavlov, & Sanwal 2004; Gotthelf et al. 2005), possibly belong to a separate subclass. Table 5 also lists the six Galactic AXPs which have been observed in the optical and/or NIR, plus one AXP found in the SMC (CXOU J0100−7211). For these six CCOs and seven AXPs, Table 6 lists observed pulsation periods (where detected), estimated ages (either the associated remnant age or spin-down age), estimated distance, $N_{\rm H}$ column density, observed (absorbed) 0.5–10 keV, H, and $K_s$ band fluxes, and estimated X-ray (2–10 keV), H, and $K_s$ luminosities[7].

As shown in Tables 5 and 6, our new J and H magnitudes limits for a Cas A XPS counterpart are about 2 magnitudes deeper than the deepest previous CCO or AXP searches. Our NICMOS J and H band magnitudes limits for the XPS are about 4 magnitudes deeper than previous searches for a Cas A XPS counterpart (see Table 1) and about 2 magnitudes deeper than currently possible from 8 – 10 m ground-based telescopes. However, a K band limit of $\sim 22-23$ mag, about $1-2$ mag deeper than the 21.2 mag limit set by Kaplan et al. (2001), is feasible using 8 – 10 m telescopes and exposures of several hours.

In terms of extinction-corrected luminosities, we reached the deepest NIR luminosity limit in the H band. Our limit of $L_{\rm H} \leq 0.3 \times 10^{30}$ erg s$^{-1}$ is about an order of magnitude lower than the luminosities (or luminosity limits) of the AXPs observed in the H band. However, the X-ray luminosity of the Cas A XPS for the column density insensitive 2–10 keV energy range is also well below those seen for most AXPs yet is not unlike other CCOs in relatively young remnants.

The origin of the NIR/optical emission in AXPs is unknown. Although some hypotheses have been suggested in the framework of the magnetar model (Thompson, Lyutikov, & Kulkarni 2002; Eichler, Gedalin, & Lyubarsky 2002), they do not give quantitative predictions for IR or optical emission levels. However, the recently observed correlations between the X-ray and NIR luminosities in some variable AXPs (most notably in 1E 2259+586; see Tam et al. 2004) suggest that the NIR radiation and X-ray radiation may be somehow related, and the NIR luminosity is a certain fraction, $\sim 10^{-4} - 10^{-3}$, of the X-ray luminosity. On the other hand, Durant & van Kerkwijk (2005a) did not find such a correlation for the AXP 1E 1048−5937.

For the Cas A XPS, the upper limit $L_{\rm Ks}/L_{\rm X} \leq 1.7 \times 10^{-3}$ is still above the values of this ratio for the $K_s$ band detected AXPs. The H band limit, $L_{\rm H}/L_{\rm X} \leq 4 \times 10^{-4}$, is a factor of 3 lower than the $L_{\rm H}/L_{\rm X}$ value for J1708−4009, but the identification of the NIR counterpart of this AXP remains uncertain (Durant & van Kerkwijk 2005a). Nearly simultaneous X-ray and NIR observations of the variable XTE J1810−197 (Rea et al. 2004) showed $L_{\rm H}/L_{\rm X} \approx 0.5 \times 10^{-4}$, a factor of 8 lower than for the XPS upper limit. For 1E 1048−5937, another X-ray and NIR variable AXP, this ratio is apparently variable. Using the H band flux from the Magellan observation of 2001 March 24 (Wang & Chakrabarty 2002b) and X-ray flux from the *XMM-Newton* observation of 2000 December 28 (Mereghetti et al. 2004), we obtain $L_{\rm H}/L_{\rm X} \approx 1 \times 10^{-3}$, while only an upper limit of $\lesssim 5 \times 10^{-4}$ can be inferred from nearly simultaneous VLT and *XMM-Newton* observations of 2004 June (Durant & van Kerkwijk 2005a; Mereghetti et al. 2004).

Thus, although it is currently unclear how universal the NIR-to-X-ray luminosity ratio is for AXPs, our deep $L_{\rm H}/L_{\rm X}$ limit is comparable with the luminosity ratios observed in AXPs. Perhaps more conclusive results would be obtained from the comparison of the $L_{\rm K}/L_{\rm X}$ ratios after much deeper K band observations of the Cas A XPS are carried out. If such future observations detect the XPS, and the NIR-to-X-ray luminosity ratio turns out to be in the same range as for AXPs, it would be a strong evidence that these objects are indeed related.

A direct comparison of the spectral energy distributions for the Cas A's XPS, the AXP 1E 2259+586 in the SNR CTB 109, and PSR B0656+14 is shown in Figure 3 along with the measured optical and NIR flux detections or limits. We see that both the XPS and the AXP have similar thermal components of the blackbody+power-law X-ray spectral models (but the AXP's thermal component is much brighter because of a larger emitting area), both being hotter than the two thermal components of the pulsar's spectrum. The extrapolations of the XPS's and AXP's thermal components into the optical domain are well below the observed fluxes or flux upper limits, while such an extrapolation matches the observed UV spectrum of the pulsar. The extrapolation of the pulsar's X-ray nonthermal (power-law) component approximately matches the observed NIR-optical spectrum, contrary to the much softer AXP's power-law component. The slope (and even the presence) of such a component in the XPS's spectrum is very uncertain (see §4); if present, its NIR-optical extrapolation also lies above the observed upper limits. Obviously, the broadband (NIR through X-rays) spectrum of 1E 2259+586 (and other AXPs) cannot be described by a simple model. Moreover, the discrepancy between the X-ray and NIR spectra suggests that even the generally adopted blackbody+power-law model for the X-ray spectrum may not be adequate. The nature of the Cas A's XPS broadband spectrum is even less clear, given the lack of detections in the NIR-optical and the uncertainty of its hard X-ray tail caused by the CCD pile-up. What is clear, however, is that the data currently available cannot rule out the hypothesis that CCOs and AXPs, being different from the commonly known radio and $\gamma$-ray pulsars, are related.

Although CCOs, including the Cas A's XPS, are the stellar remnants of core-collapse supernovae, the mass range and possibly binarity of the SN progenitor leading to their formation is unclear. The presence of CCOs in the high mass, core-collapse SNRs of Puppis A and Cas A with similar properties is intriguing given both remnants' relatively young ages (cf. Table 6) and similar ejecta kinematics and abundances. Both remnants show high-velocity, oxygen-rich ejecta and have considerable amounts of surrounding CSM material rich in nitrogen suggestive of a high mass loss episode just prior to explosion like that from a fairly high mass, WR star progenitor (Fesen, Becker, & Blair 1987).

[7] We chose the H and $K_s$ NIR bands and the 2–10 keV X-ray band as they are less sensitive to the poorly known interstellar extinction.

This leads to the question of why don't other young, high mass, O-rich core-collapse SNRs also possess similar CCOs? The 1–2 kyr old, O-rich SMC remnant 1E 0102−72 shows no CCO, but this may simply be a problem of detection difficulty due to its greater distance. Similarly, for the recently discovered but much older O-rich SMC remnant, 0103−72.6 (Park et al. 2003), the presence of considerable X-ray emission near the remnant center might prevent a clear CCO detection, much like what happened in the case of Cas A before *Chandra*'s improved resolution became available. However, the relatively young oxygen-rich Galactic and LMC remnants, G292.0+1.8 and 0540−69.3, do show bright, rapidly spinning pulsars ($P$ = 135 ms and 50 ms, respectively; Camilo et al. 2002; Seward, Harnden, & Helfand 1984; Manchester et al. 1993) and both have extensive pulsar wind nebulae. Currently, we do not understand which properties of the apparently similar progenitors predetermine the nature of the compact remnant, a CCO, or an active pulsar of the SN explosion.

In the end, a key element in our understanding of the nature of the Cas A CCO, the Puppis A CCO, and similar objects will be determining their periodicity as well as an accurate measurement of their X-ray spectra. While the data frame time employed for the recent 1 Ms *Chandra* observation of Cas A may not be useful in investigating periods $\lesssim 10$ s and obtaining a clean source spectrum, specially designed future X-ray observations of Cas A may help to find a shorter period and obtain an accurate X-ray spectrum. In the NIR-optical range, much deeper K band observations are possible. Such X-ray and NIR observations of Cas A may finally resolve the nature of its XPS and thus other compact stellar remnants as well.

We thank M. Hammell for help with the optical coordinate matching, P. Plucinsky, T. Aldcroft, and M. Juda for assistance and guidance with measuring the XPS position on *Chandra* ACIS and HRC images, and Al Schultz for help with reduction and analysis of the NICMOS data. Support for this work was provided by NASA through grant numbers GO-8692 and GO-9798 from the Space Telescope Science Institute, which is operated by AURA, Inc., under NASA contract NAS5-26555. The work of G.G.P. and D.S. was also partially supported by NASA grant NAG5-10865.

REFERENCES

Alpar, M. A. 2001, ApJ, 554, 1245
Aschenbach, B. 1999, IAU Circ. 7249
Bohlin, R.C., Savage, B.D., & Drake, J. F. 1978, ApJ, 224, 132
Camilo, F., Manchester, R. N., Gaensler, B. M., Lorimer, D. R., & Sarkissian, J. 2002, ApJ, 567, L71
Cassam-Chenaï, G., Decourchelle, A., Ballet, J., Sauvageot, J.-L., Dubner, G., & Giacani, E. 2004, A&A, 427, 199
Chatterjee, P., Hernquist, L., & Narayan, R. 2000, ApJ, 534, 373
Chakrabarty, D., Pivovaroff, M. J., Hernquist, L. E., Heyl, J. S., & Narayan, R. 2001 ApJ, 548, 800
Chevalier, R. A., & Kirshner, R. P. 1978, ApJ, 219, 931
Chevalier, R. A., & Kirshner, R. P. 1979, ApJ, 233, 154
Douvion, T., Lagage, P.O., & Césarsky, C. J. 1999, A&A, 352, L111
Duncan, R. C., & Thompson, C. 1992, ApJ, 392, L9
Durant, M. 2005, preprint (astro-ph/0506288)
Durant, M., van Kerkwijk, M. H., & Hulleman, F. 2004, in Young Neutron Stars and Their Environments, IAU Symp. 218, ed. F. Camilo & B. M. Gaensler (San Francisco: ASP), 251
Durant, M., & van Kerkwijk, M. H. 2005a, preprint (astro-ph/0502027)
Durant, M., & van Kerkwijk, M. H. 2005b, preprint (astro-ph/0506512)
Eichler, D., Gedalin, M., & Lyubarsky, Y. 2002, ApJ, 578, L121
Ekşı, K. Y., & Alpar, M. A. 2003, ApJ, 599, 450
Ekşı, K. Y., Hernquist, L., & Narayan, R. 2005, preprint (astro-ph/0501551)
Fesen, R. A., Becker, R. H., & Blair, W. P. 1987, ApJ, 313, 378
Fesen, R. A., Morse, J., Chevalier, R. A., et al. 2001, ApJ
Fesen, R. A.,, Chevalier, R. A., Holt, S. S., & Tananbaum, H. 2002, ASP Conf. Ser. 271: Neutron Stars in Supernova Remnants, eds. P.O. Slane & B. Gaensler, p 305
Gaensler, B. M. 2004, Advances in Space Research, 33, 645
Gerardy, C. L., & Fesen, R. A. 2001, AJ, 121, 2781
Gotthelf, E. V., Halpern, J. P., Buxton, M., & Bailyn, C. 2004, ApJ, 605, 368
Gotthelf, E.V. 2004, in Young Neutron Stars and Their Environments, IAU Symp. #218, ed. F. Camilo & B. M. Gaensler (San Francisco: ASP), p225
Gotthelf, E. V., Halpern, J. P., & Seward, F. D. 2005, preprint (astro-ph/0503424)
Helfand, D. J., Becker, R. H., Hawkins, G., & White, R. L. 1994, ApJ, 434, 627
Hulleman, F., van Kerkwijk, M. H., & Kulkarni, S.R. 2000, Nature, 408, 689
Hulleman, F., van Kerkwijk, M. H., & Kulkarni, S.R. 2004, A&A, 416, 1037
Hulleman, F., Tennant, A. F., van Kerkwijk, M. H., Kulkarni, S. R., Kouveliotou, C., & Patel, S. K. 2001, ApJ, 563, L49
Hurford, A. P., & Fesen, R. A. 1996, ApJ, 469, 246
Hughes, J. P., Rakowski, C. E., Burrows, D. N., & Slane, P. O. 2000, ApJ, 528, L109
Hwang, U. et al. 2004, ApJ, 615, L117
Hwang, U., & Laming, J. M. 2002, ApJ597, 362
Ibrahim, A. I., et al. 2004, ApJ, 609, L21
Israel, G. L., Covino, S., Stella, L., Campana, S., Haberl, F., & Mereghetti, S. 1999, ApJ, 518, L107
Israel, G. L., et al. 2002, ApJ, 580, L143
Israel, G. L., et al. 2003, ApJ, 589, L93
Israel, G. L., et al. 2004, ApJ, 603, L97
Jansen, F., Smith, A., Bleeker, J. A. M., de Korte, P. A. J, Peacock, A., & White, N. E. 1988, ApJ, 331, 949
Kamper, K. & van den Bergh, S. 1976, ApJS, 32, 351
Kaplan, D. L, Kulkarni, S. R., & Murray, S. S. 2001, ApJ, 558, 270
Kargaltsev, O. & Pavlov, G. G., 2005, ApJ, to be submitted
Kaspi, V. M., Gavriil, F. P., Woods, P. M., Jensen, J. B., Roberts, M. S. E., & Chakrabarty, D. 2003, ApJ, 588, L93
Keohane, J. W., Rudnick, L., & Anderson, M. C. 1996, ApJ, 466, 309
Krause, O. et al. 2005, Science, 308, 1604
Lamb, R. C., Fox, D. W., Macomb, D. J., & Prince, T. A. 2002, ApJ, 574, L29
Langer, N., & El Eid, M. F. 1986, A&A, 167, 265
Lagage, P. O., Claret, A., Ballet, J., Boulanger, F., Césarsky, C. J., Césarsky, D., Fransson, C., & Pollock, A. 1996, A&A, 315, L273
Lazendic, J. S., Slane, P. O., Gaensler, B. M., Plucinsky, P. P., Hughes, J. P., Galloway, D. K., & Crawford, F. 2003, ApJ, 593, L27
Lorimer, D. R., Lyne, A. G., & Camilo, F. 1998, A&A, 331, 1002
Manchester, R. N., Mar, D. P., Lyne, A. G., Kaspi, V. M., & Johnston, S. 1993, ApJ, 403, L29
McGarry, M. B., Gaensler, B. M., Ransom, S. M., Kaspi, V. M., & Veljkovik, S. 2005, preprint (astro-ph/0504360)
McLaughlin, M. A., Cordes, J. M., Deshpande, A. A., Gaensler, B. M., Hankins, T. H., Kaspi, V. M., & Kern, J. S. 2001, ApJ, 547, L41
Mereghetti, S., Mignani, R. P., Covino, S., Chaty, S., Israel, G. L., Neuhäuser, R., Plana, H., & Stella, L. 2001, MNRAS, 321, 143
Mereghetti, S., Chiarlone, L., Israel, G. L., & Stella, L. 2002, Neutron Stars, Pulsars, and Supernova Remnants, 29
Mereghetti, S., Tiengo, A., Israel, G. L. 2002, ApJ, 569, 275
Mereghetti, S., Tiengo, A., Stella, L., Israel, G. L., Rea, N., Zane, S., & Oosterbroek, T. 2004, ApJ, 608, 427

Moody, K., Pavlov, G. G., & Sanwal, D 2005, ApJ, to be submitted
Monet, D. E. A., et al., 1998, The USNO-A2.0 Catalogue (Washington, DC: USNO)
Murray, S. S., Ranson, S. M., Juda, M., Hwang, U., & Holt, S. S. 2002, ApJ, 566, 1039
Nakamura, T., Mazzali, P. A., Nomoto, K., & Iwamoto, K. 2001, ApJ, 550, 991
Nazé, Y., Hartwell, J. M., Stevens, I. R., Manfroid, J., Marchenko, S., Corcoran, M. F., Moffat, A. F. J., & Skalkowski, G. 2003, ApJ, 586, 983
Park, S., Hughes, J. P., Burrows, D. N., Slane, P. O., Nousek, J. A., & Garmire, G. P. 2003, ApJ, 598, L95
Patel, S. K., et al. 2001, ApJ, 563, L45
Pavlov, G. G., & Zavlin, V. E. 1999, IAU Circ. 7270
Pavlov, G. G., Zavlin, V. E., Aschenbach, B., Trümper, J., & Sanwal, D. 1999, preprint (astro-ph/9912024)
Pavlov, G. G., Zavlin, V. E., Aschenbach, B., Trümper, J., & Sanwal, D. 2000, ApJ, 531, L53
Pavlov, G. G., Sanwal, D., Kiziltan, B., & Garmire, G. 2001, ApJ, 559, L131
Pavlov, G. G., Sanwal, D., Garmire, G. P., & Zavlin, V. E. 2002a, in Neutron Stars in Supernova Remnants, ed. P. O. Slane & B. M. Gaensler, ASP Conf. Ser. 271 (San Francisco: ASP), 247
Pavlov, G. G., Zavlin, V. E., & Sanwal, D. 2002b, Proc. 270 WE-Heraeus Seminar on Neutron Stars, Pulsars, and Supernova Remnants, ed. W. Becker, H. Lesch, & J. Trümper (Garching: MPE), 273
Pavlov, G. G., Sanwal, D., & Teter, M. A. 2004, in Young Neutron Stars and Their Environments, IAU Symp. 218, ed. F. Camilo & B. M. Gaensler (San Francisco: ASP), 239
Pellizzoni, A., Mereghetti, S., & De Luca, A. 2002, A&A, 393, L65
Perna, R., Hernquist, L., & Narayan, R. 2000, ApJ, 541, 344
Petre, R., Becker, C. M., & Winkler, P. F. 1996, ApJ, 465, L43
Predehl, P., & Schmitt, J. H. M. M. 1995 A&A, 293, 889
Ransom, S. M. 2002, in Neutron Stars in Supernova Remnants, ASP Conf. Ser., v.271, eds. P. O. Slane & B. M. Gaensler (San Francisco: ASP), 361
Rea, N., et al. 2004, A&A, 425, L5
Reed, J. E., Hester, J. J., Fabian, A. C., & Winkler, P. F. 1995, ApJ, 440, 706
Rejkuba, M., Minniti, D., & Gregg, M. D., et al. 2000, AJ, 120, 801
Reynoso, E. M., & Goss, W. M. 2002, ApJ, 575, 871
Rothschild, R. E. & Lingenfelter, R. E. 2003, ApJ, 582, 257
Ryan, E., Wagner, R. M., & Starrfield, S. G. 2001, ApJ, 548, 811
Sasaki, M., Plucinsky, P. P., Gaetz, T. J., Smith, R. K., Edgar, R. J., & Slane, P. O. 2004, ApJ, 617, 322
Seward, F. D., Harnden, F. R., & Helfand, D. J. 1984, ApJ, 287, L19
Seward, F. D., Slane, P. O., Smith, R. K., & Sun, M. 2003, ApJ, 584, 414
Sollerman, J., et al. 2002, A&A, 386, 944
Tam, C. R., Kaspi, V. M., van Kerkwijk, M. H., & Durant, M. 2004, ApJ, 617, L53
Tananbaum, H. 1999, IAU Circ. 7246
Teter, M. A., Pavlov, G. G., Tsuruta, S., & Liebmann, A. 2004, BAAS, 204, 7413
Teter, M. A., Pavlov, G. G., Sanval, D., & Tsuruta, S. 2005, ApJ, to be submitted
Thompson, C. & Duncan, R. C. 1996, ApJ, 473, 322
Thompson, C. R., Lyutikov, M., & Kulkarni, S. 2002, ApJ, 574, 332
Troland, T. H., Crutcher, R. M., & Heiles, C. 1985, ApJ, 298, 808
Thorstensen, J. R., Fesen, R. A., & van den Bergh, S. 2001 AJ, 122, 297
Tsunemi, H., Yamashita, K. Masai, K., Hayakawa, S., & Koyama, K. 1986, ApJ, 306, 248
van den Bergh, S., & Kamper, K. W. 1983, ApJ, 268, 129
van den Bergh, S., & Pritchet, C. J. 1986 ApJ, 307, 723
van Paradijs, J., & McClintock, J. E. 1995, X-ray Binaries, eds. W.H.G. Lewin, J. van Paradijs,
van Paradijs, J., Taam, R. E., & van den Heuvel, E. P. J. 1995, A&A, 299 L41
Wachter, S., et al. 2004, ApJ, 615, 887
Wang, Z., & Chakrabarty, D. 2002a, ASP Conf. Ser. 271: Neutron Stars in Supernova Remnants, eds. P.O. Slane & B. Gaensler, p 297
Wang, Z., & Chakrabarty, D. 2002b, ApJ, 579, L33
Willingale, R., Bleeker, J. A. M., van der Heyden, K. J., Kaastra, J. S., & Vink, J. 2002, å, 381, 1039
Woan, G., & Duffett-Smith, P.J. 1993, MNRAS, 260, 693
Woods, P. M., & Thompson, C. 2004, preprint (astro-ph/0406133)
Zharikov, S., Shibanov, Yu., & Komarova, V. 2004, Adv. Space Res., submitted (astro-ph/0410152)
Zavlin V. E., & Pavlov, G. G. 2004, ApJ, 616, 452
Zavlin, V. E., Pavlov, G. G., Sanwal, D., & Trümper, J. 2000, ApJ, 540, L25
Zavlin, V. E., Pavlov, G. G., & Sanwal, D. 2004, ApJ, 606, 444

TABLE 1
Optical and Near-Infrared Magnitude Limits for the Cas A XPS

| Reference | R | F675W | J | H | K |
|---|---|---|---|---|---|
| van den Bergh & Pritchet (1986) | $\geq$24.8 | ··· | ··· | ··· | ··· |
| Ryan et al. (2001) | $\geq$26.3 | ··· | ··· | ··· | ··· |
| Kaplan et al. (2001) | $\geq$25.0 | $\geq$27.3 | $\geq$22.5 | $\geq$20 | $\geq$21.2 |
| Fesen et al. (2002) | $\geq$27.8[a] | $\geq$28.9[a] | ··· | ··· | ··· |
| This work | ··· | ··· | $\geq$26.2[b] | $\geq$24.6[c] | ··· |
| Ground-based NIR limits[d] | ··· | ··· | ∼23.6 | ∼22.8 | ∼22.3 |

[a]Estimated value from the 50CCD STIS image.
[b]F110W magnitude limit.
[c]F160W magnitude limit.
[d]Magnitude limits that could be reached in a one hour exposure (without adaptive optics) using Subaru's IRCS in 0.″5 seeing.

TABLE 2
Coordinates of the Cas A X-Ray Point Source (XPS)

| Reference | Source | $\alpha$(J2000) | $\delta$(J2000) |
|---|---|---|---|
| Tananbaum (1999) | ACIS-S ObsID 0214 | $23^h\ 23^m\ 27\overset{s}{.}940 \pm 0\overset{s}{.}30$ | $58°\ 48'\ 42\overset{''}{.}40 \pm 2\overset{''}{.}5$ |
| Kaplan et al. (2001) | ACIS + HRC | $23^h\ 23^m\ 27\overset{s}{.}857 \pm 0\overset{s}{.}13$ | $58°\ 48'\ 42\overset{''}{.}77 \pm 1\overset{''}{.}0$ |
| Murray et al. (2002) | HRC-S ObsID 1857 | $23^h\ 23^m\ 27\overset{s}{.}920 \pm 0\overset{s}{.}13$ | $58°\ 48'\ 42\overset{''}{.}55 \pm 1\overset{''}{.}0$ |
| This work | HRC-S ObsID 1038 | $23^h\ 23^m\ 27\overset{s}{.}957 \pm 0\overset{s}{.}08$ | $58°\ 48'\ 42\overset{''}{.}53 \pm 0\overset{''}{.}6$ |
| " " | HRC-I ObsID 1505 | $23^h\ 23^m\ 27\overset{s}{.}932 \pm 0\overset{s}{.}08$ | $58°\ 48'\ 42\overset{''}{.}57 \pm 0\overset{''}{.}6$ |
| " " | HRC-S ObsID 1857 | $23^h\ 23^m\ 27\overset{s}{.}961 \pm 0\overset{s}{.}08$ | $58°\ 48'\ 42\overset{''}{.}62 \pm 0\overset{''}{.}6$ |
| " " | ACIS-S ObsID 5196 | $23^h\ 23^m\ 27\overset{s}{.}921 \pm 0\overset{s}{.}08$ | $58°\ 48'\ 42\overset{''}{.}46 \pm 0\overset{''}{.}6$ |
| " " | ACIS-S ObsID 5319 | $23^h\ 23^m\ 27\overset{s}{.}913 \pm 0\overset{s}{.}08$ | $58°\ 48'\ 42\overset{''}{.}34 \pm 0\overset{''}{.}6$ |
| " " | ACIS-S VLP + Optical | $23^h\ 23^m\ 27\overset{s}{.}945 \pm 0\overset{s}{.}08$ | $58°\ 48'\ 42\overset{''}{.}45 \pm 0\overset{''}{.}6$ |
| Adopted XPS position | | $23^h\ 23^m\ 27\overset{s}{.}943 \pm 0\overset{s}{.}05$ | $58°\ 48'\ 42\overset{''}{.}51 \pm 0\overset{''}{.}4$ |

TABLE 3
Point sources on 1 Ms VLP *Chandra* ACIS-S image of Cas A

| Star ID | $\alpha$(J2000) | $\delta$(J2000) | R mag | B mag |
|---|---|---|---|---|
| Manually matched USNO-2.0 stars | | | | |
| USNO 2.0 U1425-15020099 | $23^h\ 23^m\ 26\overset{s}{.}33$ | $58°\ 53'\ 10\overset{''}{.}1$ | 18.1 | 20.2 |
| USNO 2.0 U1425-15018830 | $23^h\ 23^m\ 22\overset{s}{.}78$ | $58°\ 52'\ 49\overset{''}{.}4$ | 11.7 | 12.5 |
| USNO 2.0 U1425-15027102 | $23^h\ 23^m\ 45\overset{s}{.}81$ | $58°\ 50'\ 48\overset{''}{.}7$ | 12.9 | 14.3 |
| Sources matching USNO-2.0 catalog | | | | |
| USNO 2.0 U1425-15007635 | $23^h\ 22^m\ 51\overset{s}{.}55$ | $58°\ 50'\ 19\overset{''}{.}6$ | 14.8 | 16.5 |
| USNO 2.0 U1425-15012096 | $23^h\ 23^m\ 03\overset{s}{.}84$ | $58°\ 49'\ 18\overset{''}{.}2$ | 14.9 | 16.3 |
| USNO 2.0 U1425-15012463 | $23^h\ 23^m\ 04\overset{s}{.}82$ | $58°\ 48'\ 00\overset{''}{.}1$ | 14.2 | 15.3 |
| Sources matching non-USNO stars | | | | |
| MDM ID 1093 | $23^h\ 23^m\ 43\overset{s}{.}16$ | $58°\ 52'\ 24\overset{''}{.}7$ | 12.8 | ··· |
| MDM ID 1070 | $23^h\ 23^m\ 41\overset{s}{.}76$ | $58°\ 52'\ 27\overset{''}{.}3$ | 19.5 | ··· |
| MDM ID 1315 | $23^h\ 23^m\ 57\overset{s}{.}17$ | $58°\ 48'\ 12\overset{''}{.}1$ | 21.2 | ··· |

TABLE 4
Optical and Near-IR Sources Near the Cas A X-Ray Point Source (XPS)

| Object | $\alpha$(J2000) | $\delta$(J2000) | $\Delta r$ | STIS[a] | R | F110W | F160W | $K_s$ |
|---|---|---|---|---|---|---|---|---|
| XPS | $23^h23^m27^s.943 \pm 0^s.05$ | $58°48'42''.51 \pm 0''.4$ | $0''.0$ | $\geq 28.5$ | $\geq 27.8$ | $\geq 26.2$ | $\geq 24.6$ | $\geq 21.2$[b] |
| Star A | $23^h23^m27^s.752 \pm 0^s.012$ | $58°48'41''.51 \pm 0''.1$ | $1''.8$ | 26.4±0.1 | 25.7±0.2[c] | 21.9±0.1 | 20.6±0.1 | 20.5±0.3 |
| Star B | $23^h23^m27^s.938 \pm 0^s.025$ | $58°48'40''.59 \pm 0''.2$ | $1''.9$ | $\geq 28.5$ | $\geq 27.8$ | 24.7±0.2 | 23.0±0.2 | ··· |
| Star C | $23^h23^m28^s.075 \pm 0^s.020$ | $58°48'45''.92 \pm 0''.1$ | $3''.6$ | $\geq 28.5$ | $\geq 27.8$ | 25.6±0.2 | 23.7±0.2 | ··· |
| Star 1 | $23^h23^m27^s.170 \pm 0^s.012$ | $58°48'40''.25 \pm 0''.1$ | $6''.5$ | 23.6±0.1 | 22.9±0.3 | 19.1±0.1 | 17.4±0.1 | 17.5±0.2[d] |
| Star 2 | $23^h23^m27^s.215 \pm 0^s.012$ | $58°48'46''.84 \pm 0''.1$ | $7''.1$ | 25.4±0.1 | 24.7±0.3[e] | 20.4±0.1 | 18.4±0.1 | 18.4±0.2[d] |

[a]STIS 50CCD magnitudes.
[b]Magnitude from Kaplan et al. (2001).
[c]Magnitude based on WFPC2 F675W image Kaplan et al. (2001).
[d]Magnitude based on measurements of K band image of Cas A from Gerardy & Fesen (2001).
[e]Magnitude from Ryan et al. (2001).

TABLE 5
Observed Optical and Near IR Magnitudes for Radio-Quiet Neutron Stars

| Object | SNR | $R$ (mag) | $J$ (mag) | $H$ (mag) | $K_s$ (mag) | Refs. |
|---|---|---|---|---|---|---|
| CCOs | | | | | | |
| Cas A XPS | G111.7−2.1 (Cas A) | ≥27.8 | ≥26.2[a] | ≥24.6[a] | ≥21.2 | 1–4 |
| CXOU J0852−4617 | G266.2−1.2 (Vela Junior) | ≥22.0 | ··· | ··· | ··· | 5, 6 |
| 1WGA J1713−3949 | G347.3−0.5 | ··· | ··· | ··· | ··· | 7 |
| RX J0822−4300 | G260.4−3.4 (Puppis A) | ≥24.8 | ··· | ··· | ··· | 8, 9 |
| 1E 1207−5209[b] | G296.5+10.0 (PKS 1209−51/52) | ≥26.6 | ≥23.5 | ≥22.4 | ≥22.0 | 10 |
| RX J1853+0040 | G33.6+0.1 (Kes 79) | ≥24.9 | ··· | ··· | ··· | 11, 12 |
| AXPs | | | | | | |
| XTE J1810−197 | ··· | ≥21.5 | ≥23.0 | 22.0–22.7[c] | 20.8–21.4[c] | 13–16 |
| 1E 1048−5937 | ··· | ≥24.8 | 21.7–23.4[c] | 20.8–(≥21.5)[c] | 19.4–21.3[c] | 17–20 |
| 1E 1841−045 | G27.4+0.0 (Kes73) | ≥23.0 | ≥22.1 | ≥20.7 | ≥19.9 | 21–23 |
| CXOU J0100−7211[d] | ··· | 24.2[e] | ··· | ··· | ··· | 24–27 |
| 1RXS J1708−4009[d] | ··· | ≥26.5 | 20.9 | 18.6;18.85[f] | 18.3;17.5[f] | 28 |
| 4U 0142+614 | ··· | 24.9 | ··· | ··· | 19.7–20.2[c] | 29,30 |
| 1E 2259+586 | G109.1−1.0 (CTB 109) | ≥26.4 | ≥23.8 | ··· | 20.4–21.7[c] | 31–34 |

[a]$m_{\rm F110W} \approx J$; $m_{\rm F160W} \approx H$.
[b]Moody, Pavlov, & Sanwal (2005) detected an M dwarf in the *Chandra* error circle, with $J = 21.7$, $H = 21.2$, and $K_s = 20.7$. The magnitudes in table are $3\sigma$ detection limits from that observation.
[c]Source variable.
[d]Proposed counterpart unconfirmed
[e]$m_{\rm F606W}$ based on *HST* WFPC2 observations.
[f]Israel et al. (2004) quote different magnitudes from NTT ($H$ and $K_s$) and CFHT ($H$ and $K'$) data.

References – 1: Kaplan et al. (2001), 2: Ryan, Wagner, & Starrfield (2001) 3: Fesen et al. (2002), 4: this work, 5: Pavlov et al. (2001), 6: Pellizzoni, Mereghetti, & De Luca (2002), 7: Cassam-Chenaï et al. (2004) 8: Petre, Becker, & Winkler (1996), 9: Wang & Chakrabarty (2002a), 10: Moody, Pavlov, & Sanwal (2005), 11: Seward et al. (2003), 12: Gotthelf et al. (2005), 13: Israel et al. (2004), 14: Gotthelf et al. (2004), 15: Ibrahim et al. (2004), 16: Rea et al. (2004), 17: Wang & Chakrabarty (2002b), 18: Israel et al. (2002), 19: Durant et al. (2004), 20: Durant & van Kerkwijk (2005a) 21: Mereghetti et al. (2001), 22: Wachter et al. (2004), 23: Durant (2005) 24: Lamb et al. (2002), 25: Nazé et al. (2003), 26: McGarry et al. (2005), 27: Durant & van Kerkwijk (2005b) 28: Israel et al. (2003), 29: Hulleman et al. (2000), 30: Hulleman et al. (2004), 31: Hulleman et al. (2001), 32: Kaspi et al. (2003), 33: Israel et al. (2003), 34: Tam, Kaspi, & van Kerkwijk (2004)

TABLE 6
Observed X-Ray and NIR Fluxes and Estimated Luminosities for Radio-Quiet Neutron Stars

| Object | $P$ (s) | Age[a] (kyr) | $D$ (kpc) | $N_{\rm H,22}$ | $F^{\rm obs}_{\rm X,-12}$ | $F^{\rm obs}_{\rm H,-16}$ | $F^{\rm obs}_{\rm Ks,-16}$ | $L_{\rm X,33}$ | $L_{\rm H,30}$ | $L_{\rm Ks,30}$ |
|---|---|---|---|---|---|---|---|---|---|---|
| CCOs | | | | | | | | | | |
| Cas A XPS | ··· | 0.3 | 3.4 | 1.2 | 0.8 | ≤0.7[b] | ≤5 | 0.75 | ≤0.3 | ≤1.3 |
| CXOU J0852−4617 | ··· | 1–3 | 2 | 0.4 | 1.4 | ··· | ··· | 0.29 | ··· | ··· |
| 1WGA J1713−3949 | ··· | 1–3 | 2 | 0.5 | 2.9 | ··· | ··· | 0.62 | ··· | ··· |
| RX J0822−4300 | ··· | 3–4 | 2 | 0.3 | 4.5 | ··· | ··· | 0.33 | ··· | ··· |
| 1E 1207−5209 | 0.4 | 3–20 | 2 | 0.1 | 1.9 | ≤5 | ≤2 | 0.084 | ≤0.28 | ≤0.11 |
| RX J1853+0040 | 0.1 | 5–8 | 7 | 1.5 | 0.2 | ··· | ··· | 1.1 | ··· | ··· |
| AXPs | | | | | | | | | | |
| XTE J1810−197 | 5.5 | [2.4] | 5 | 1.1 | 0.5–90 | 4–8 | 4–7 | 0.2–65 | 3–6 | 2–4 |
| 1E 1048−5937 | 6.5 | [4.3] | 3 | 1.0 | 7–30 | (≤12)–24 | 4–25 | 5–25 | (≤3)–6 | 0.8–4 |
| 1E 1841−045 | 11.8 | [4.5] | 7 | 2.5 | 20 | ≤26 | ≤15 | 110 | ≤140 | ≤35 |
| CXOU J0100−72111 | 8.0 | [6.8] | 57 | 0.3 | 1.9 | ··· | ··· | 39 | ··· | ··· |
| 1RXS J1708−4009[c] | 11.0 | [9.0] | 8 | 1.4 | 40 | 180 | 68 | 490 | 460 | 110 |
| 4U 0142+614 | 8.7 | [70] | 3 | 0.9 | 120 | ··· | 12–19 | 89 | ··· | 2–3 |
| 1E 2259+586 | 7.0 | [220] | 3 | 1.0 | 30–90 | ··· | 3–10 | 20–60 | ··· | 0.6–2 |

Note. — CCO and AXP values listed for period, age, and distances (cols. 2–4) are taken from Pavlov et al. (2002a, 2004) and Woods & Thompson (2004), with updates from the references listed in Table 5. Hydrogen column densities (col. 5) are in units of $10^{22}$ cm$^{-2}$. Observed (absorbed) X-ray flux for the 0.5–10 keV range (col. 6) and H and $K_s$ band fluxes (cols. 7–8) are in units of $10^{-12}$ erg cm$^{-2}$ s$^{-1}$ and $10^{-16}$ erg cm$^{-2}$ s$^{-1}$, respectively. Adopting the distances listed in column 4, estimated X-ray luminosities in the 2–10 keV range in units of $10^{33}$ erg s$^{-1}$ and H and $K_s$ band luminosities in units of $10^{30}$ erg s$^{-1}$ are given in columns 9–11.

[a]Ages for the CCOs are associated SNR age estimates. Age estimates for the AXPs (listed in brackets) are spin-down values taken from Woods & Thompson (2004). For J1810−197 and J0100−7211, we list estimates from Gotthelf et al. (2004) and McGarry et al. (2005), respectively. Age estimates for the two AXPs thought associated with SNRs, 1841−045 in G24.7+0.0 and 2259+586 in G109.1−1.0, are considerably larger than the SNR ages, namely, 0.5–2 kyr (Helfand et al. 1994) and 8–10 kyr (Sasaki et al. 2004), respectively.

[b]F160W ≈ H.

[c]Proposed NIR counterpart unconfirmed.

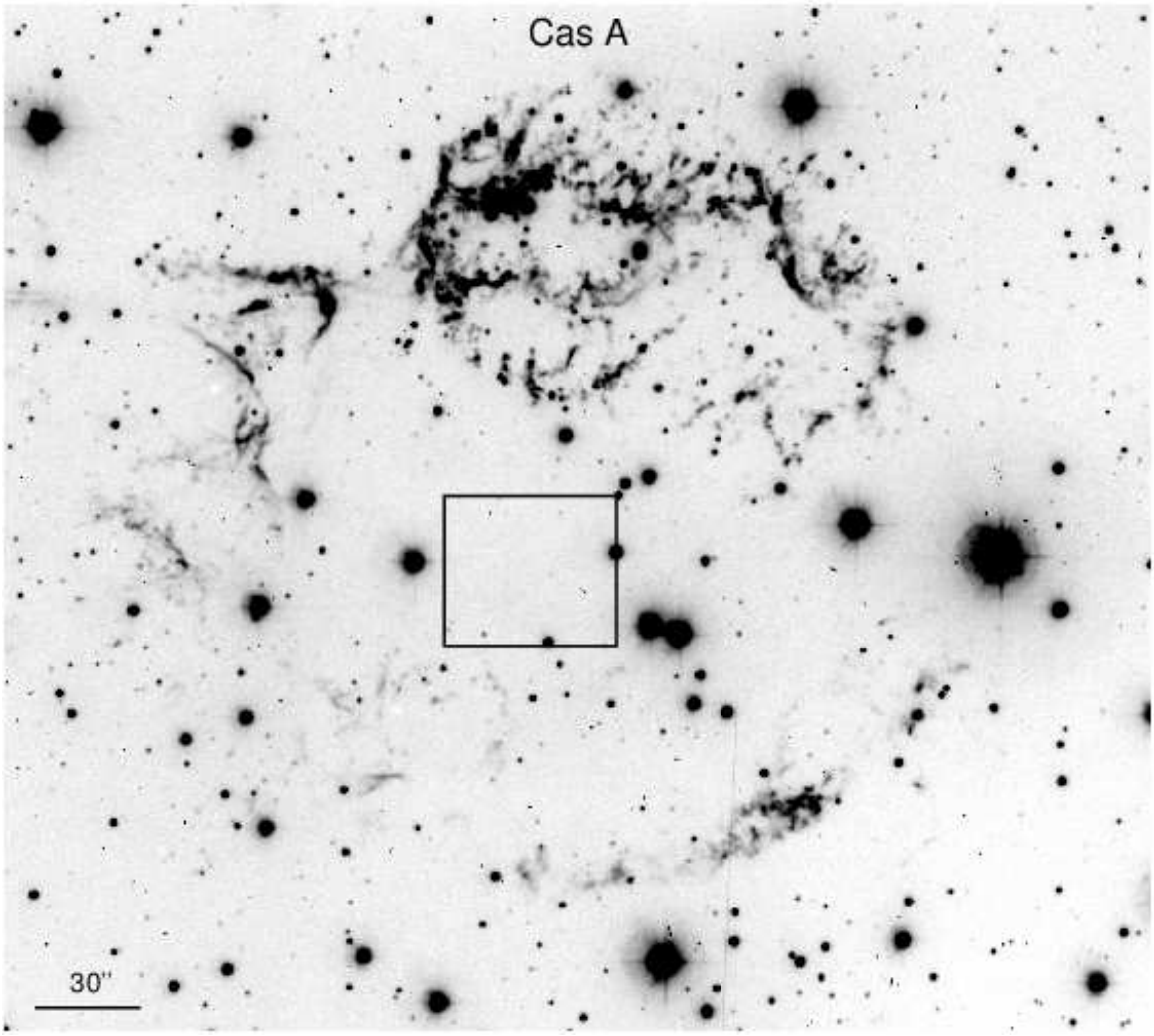


FIG. 1.— MDM R band image of Cas A with the field of view of the *HST* STIS image of the remnant's central region (shown in Fig. 2) marked.

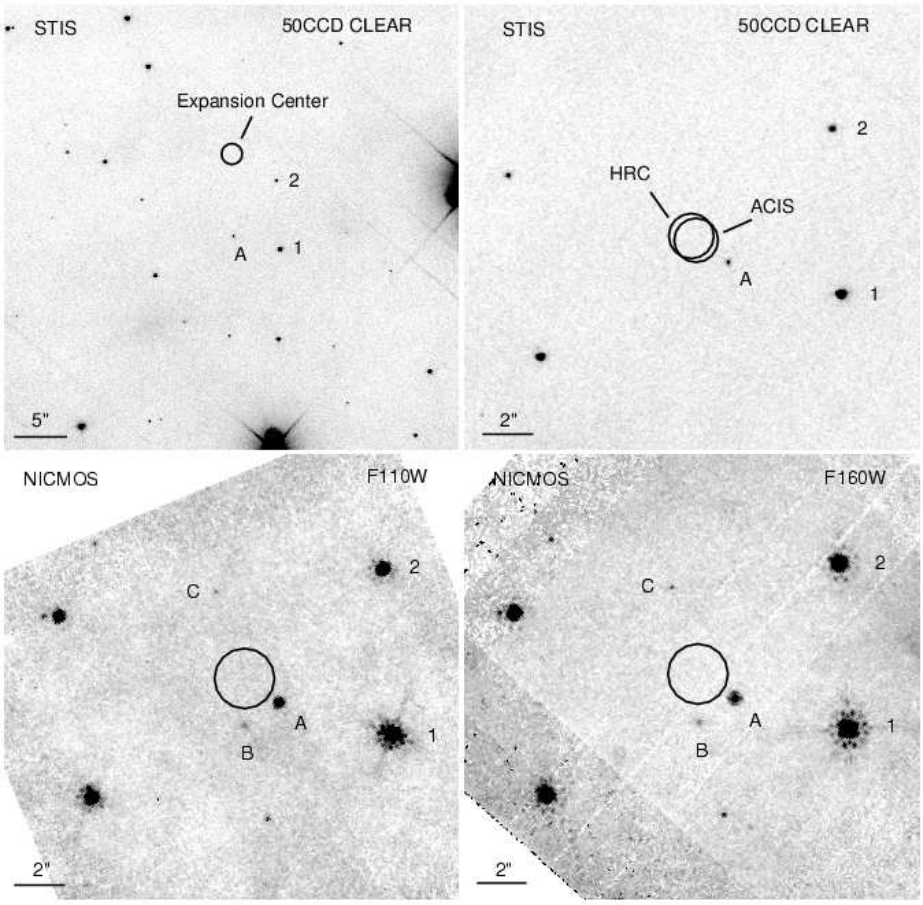


FIG. 2.— *HST* images of the Cas A central region near the X-ray point source (XPS). Upper left panel shows the 2001 STIS image of the remnant's central region with the Thorstensen et al. (2001) expansion center indicated ($\alpha = 23^{\rm h}23^{\rm m}27\overset{\rm s}{.}77 \pm 0\overset{\rm s}{.}05$, $\delta = 58^{\rm o}48'49\overset{''}{.}4 \pm 0\overset{''}{.}4$ ). Upper right panel shows an enlargement of the STIS image with the 95% confidence level circles marked for *Chandra* ACIS-S (radius = $0\overset{''}{.}9$) and HRC-S (radius = $0\overset{''}{.}9$) centered on the respective mean positions for each data set as listed in Table 2. Star 'A' lies closest to the nominal XPS position but is likely a foreground late-type star (Kaplan et al. 2001). Lower panels show NICMOS J and H band images of the Cas A central region with 99% confidence level circles (radius = $1\overset{''}{.}2$) shown centered on our adopted position for the XPS ($\alpha = 23^{\rm h}23^{\rm m}27\overset{\rm s}{.}943$, $\delta = 58^{\rm o}48'42\overset{''}{.}51$; see text and Table 2). While the NICMOS H band image revealed a few faint, additional sources (B and C) near the XPS, no source is detected within the *Chandra* error circle.

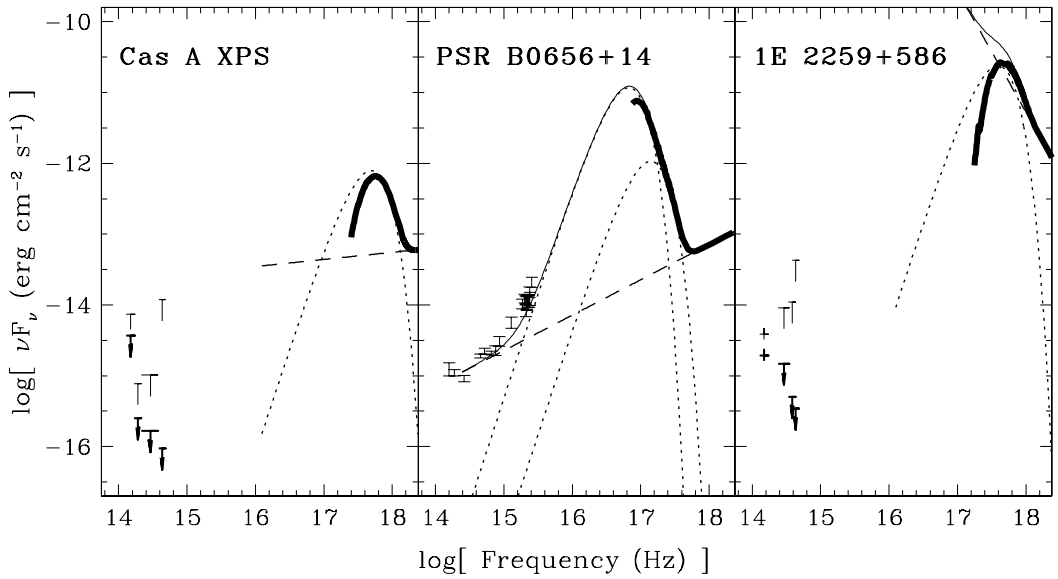


FIG. 3.— Comparisons of the broadband energy spectra of the AXP 1E 2259+586 in CTB 109, PSR B0656+14, and the Cas A XPS. Thick and thin solid curves show the observed and extinction-corrected spectra. Dotted and dashed lines show the extinction-corrected thermal and power-law components of the spectral fits, respectively (there are two thermal components in the spectrum of B0656+14). Thick and thin symbols in the NIR-optical domain correspond to the observed and extinction-corrected detections or upper limits (only the extinction-corrected points are shown for PSR B0656+14). For the variable 1E 2259+586, the X-ray spectral flux is taken from archival *Chandra* data (observed on 2000 January 11; see Patel et al. 2001) while the NIR points are from a Keck I observation of 1999 June 23/24 (Hulleman et al. 2001). The AXP was supposedly in a quiescent state during both the NIR and X-ray observations.